

Long-lived charged particles and multi-lepton signatures from neutrino mass models

Carolina Arbeláez R,^{1,*} Giovanna Cottin,^{2,†} Juan Carlos Helo,^{3,‡} and Martin Hirsch^{4,§}

¹*Universidad Técnica Federico Santa María and Centro Científico Tecnológico de Valparaíso CCTVal Casilla 110-V, Valparaíso, Chile*

²*Departamento de Ciencias, Facultad de Artes Liberales, Universidad Adolfo Ibáñez, Diagonal Las Torres 2640, Santiago, Chile*

³*Departamento de Física, Facultad de Ciencias, Universidad de La Serena, Avenida Cisternas 1200, La Serena, Chile*

⁴*Instituto de Física Corpuscular (CSIC-Universitat de València), Apdo. 22085, E-46071 Valencia, Spain*

Lepton number violation (LNV) is usually searched for by the LHC collaborations using the same-sign di-lepton plus jet signature. In this paper we discuss multi-lepton signals of LNV that can arise with experimentally interesting rates in certain loop models of neutrino mass generation. Interestingly, in such models the observed smallness of the active neutrino masses, together with the high-multiplicity of the final states, leads in large parts of the viable parameter space of such models to the prediction of long-lived *charged* particles, that leave highly ionizing tracks in the detectors. We focus on one particular 1-loop neutrino mass model in this class and discuss its LHC phenomenology in some detail.

I. INTRODUCTION

Lepton number violation (LNV) is usually searched for by the LHC collaborations using the same-sign di-lepton plus jet signature [1, 2]. This signal was first proposed in the context of the left-right symmetric model [3], but appears – at least in principle – in all Majorana neutrino mass models.¹ In this paper, we discuss multi-lepton signals, possibly accompanied by long-lived heavy particles leaving charged tracks in the LHC detectors. Here, by “multi-lepton” we understand final states with 4-, 6- or even more leptons accompanied by jets, but *without missing energy*. As we will show, this kind of exotic LNV signatures appears in specific loop models of neutrino mass generation.

From the theoretical point of view, the smallness of neutrino masses could be understood, if neutrino masses are generated radiatively. Radiative neutrino mass models have a long history [4–7], see also the recent review [8]. Different radiative models can be classified according to the topology of the diagram from which the neutrino mass is generated. Systematic classifications have been done for 1-loop [9], 2-loop [10] and even 3-loop [11] models.

Customarily, when constructing neutrino mass models, model builders use the smallest available representations to do required tasks. For example, in fig. (1) to the left we show one particular 1-loop $d = 5$ diagram, the only diagram from topology T_3 in [9]. Choosing $C = 1$, $R = 1$ and $Y = 0$ results in the *scotogenic* model [12]. This renowned neutrino mass model requires an additional Z_2 symmetry, under which the particles internal to the loop are odd, in order to avoid the tree-level type-I seesaw. But once we accept this premise, as a free bonus the scotogenic model contains two potential dark matter candidates. It should be clear, however, that a priori there is no fundamental principle that fixes (C, R, Y) in such kind of model building exercise.

Choosing instead $C = 1$, $R = 2$ and $Y = 5/2$ results in the particular model shown to the right. Different from the scotogenic model, this model variant does not need any additional symmetry (on top of the standard model gauge group) to avoid tree-level neutrino masses, i.e. the diagram shown is automatically the leading contribution to the neutrino mass matrix. More interesting for us, however, is that this model represents the proto-type for a class of neutrino mass models with multi-lepton signals at colliders, which are the subject of this paper.

Searches for LNV require signatures with *charged* leptons in the final state. In models based on the type-I seesaw [13–15], mixing between the singlet neutrinos,² N , and the active neutrinos of the standard model (SM) leads to a non-zero production cross section of these states at the LHC: $pp \rightarrow (W^\pm)^* \rightarrow l^\pm N$. The N , being a Majorana particle, can decay via $N \rightarrow l^\pm q \bar{q}$, leading to the standard $2l + jj$ signal, with both same-sign and opposite-sign leptons. CMS has performed a search for Majorana N ’s using this channel [16]. The N can also decay as $N \rightarrow l^\pm l'^\mp \nu$, which leads to

*Electronic address: carolina.arbelaez@usm.cl

†Electronic address: giovanna.cottin@uai.cl

‡Electronic address: jchelo@userena.cl

§Electronic address: mahirsch@ific.uv.es

¹ Signal rates and kinematics of this final state are of course highly model dependent.

² N appear under various names in the literature: sterile neutrinos, heavy neutrinos or also heavy neutral leptons (HNLs).

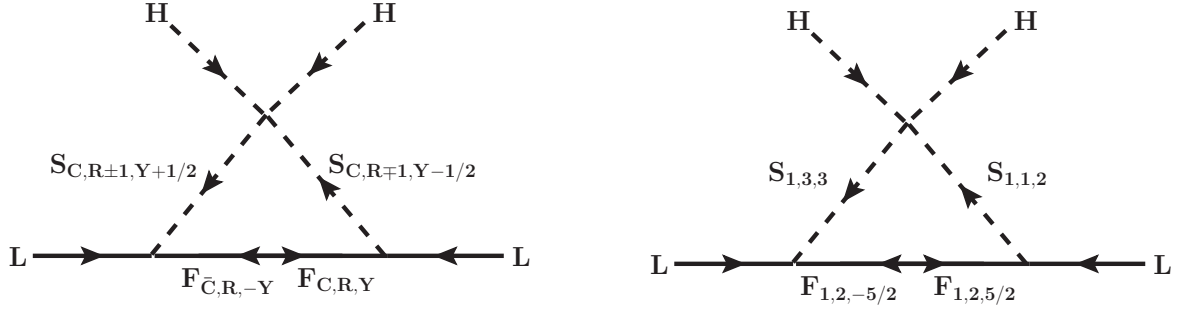


FIG. 1: To the left: The general 1-loop $d = 5$ neutrino diagram T_3 [9]. To the right: Choosing $C = 1$, $R = 2$ and $Y = 5/2$ results in the prototype model that predicts the multi-lepton LNV signals discussed in the text.

a tri-lepton signature with missing momentum in the event. CMS has used this signature to search for seesaw type-I HNLs [17], as well as for the type-III seesaw [18]. While interesting limits on new particles have been established by these searches, we need to stress, however, that events with missing energy can *never establish the existence of LNV*.

We define LNV *multi-lepton* events as final states with at least four charged leptons in the final state (with a lepton number balance of $L = \pm 2$). Consider the Feynman diagram of a process leading to $l^\pm l^\pm jj$. It is easy to add either a photon or a Z^0 boson to this diagram. Decaying $\gamma/Z^0 \rightarrow l^+ l^-$ will lead to events such as $l^\pm l^\pm (l^+ l^-) jj$, i.e. a LNV multi-lepton event in our definition. However, usually the rates for such a final state are suppressed relative to $l^\pm l^\pm jj$ by at least a factor of α and thus, experimentally uninteresting. This is different in the models discussed in this paper. In the model defined by the particles shown in fig. (1) right, multi-lepton events have actually *larger rates* than di-lepton events, as we will show below. Since such high multiplicity final states should also have less background at the LHC, we believe a dedicated search for this kind of signals at the LHC might be worthwhile.

The purpose of this paper is to study in some detail the phenomenology of the model shown in fig. (1). Since the model uses only non-singlet states, all beyond SM particles can in principle be produced at the LHC. Final states contain always at least two same-sign leptons and the model predicts final states with up to eight leptons. The model can easily fit neutrino data. Given the smallness of neutrino masses, one expects that also the decay widths of the exotic scalars are small. As we will show, this is especially so in the parts of the parameter space where $S_{1,3,3}$ is the lightest exotic particle. If this is the case, we expect the scalars from $S_{1,3,3}$ to be long-lived and leave charged tracks in the detectors before decaying.

The rest of this paper is structured as follows. In section II we will present the model and give some approximation formulas for the decay rates of the exotic particles. In section III we discuss our numerical results. In section III A we will show decay lengths of the exotic particles of our model, concentrating mostly on the scalars. In section III B we calculate cross sections and discuss the reach of the LHC for both, present and future luminosities. We then close with a more general discussion of multi-lepton signatures.

II. THE MODEL

For our numerical results, we will concentrate on a specific model variant, the neutrino mass diagram is shown in fig. (1). The model introduces a vector-like fermion pair, $(F, \bar{F}) \equiv (F_{1,2,5/2}, F_{1,2,-5/2})$. Here and everywhere else in this paper, subscripts in the gauge basis denote the transformation properties and charge under the SM gauge group in the order $SU(3)_C \times SU(2)_L \times U(1)_Y$. In the numerical implementation we use three copies of (F, \bar{F}) , one for each lepton generation. We note, however, that neutrino data could already be explained with just one copy of (F, \bar{F}) . The model also has two new scalars, $S_1 \equiv S_{1,1,2}$ and $S_3 \equiv S_{1,3,3}$.

The lagrangian of the model is given by:

$$\begin{aligned} \mathcal{L} = \mathcal{L}_{SM} & - m_F F \bar{F} - h_{ee} e^c e^c S_1^\dagger - h_F L F S_1^\dagger - h_{\bar{F}} L \bar{F} S_3 \\ & - m_{S_1}^2 |S_1|^2 - m_{S_3}^2 |S_3|^2 + \lambda_2 |H|^2 |S_1|^2 \\ & + \left(\lambda_{3a} |H^\dagger H| |S_3^\dagger S_3| + \lambda_{3b} |H S_3 H^\dagger S_3^\dagger| \right) + \lambda_4 |S_1|^4 - \lambda_5 H H S_2 S_2^\dagger \\ & + \left(\lambda_{6a} |S_3^\dagger S_3|^2 + \lambda_{6b} |S_3 S_3^\dagger S_3^\dagger| \right) + \lambda_7 |S_1|^2 |S_3|^2 \end{aligned} \quad (1)$$

The terms proportional to λ_3 and λ_6 have two independent $SU(2)_L$ contractions each. We used Sym2Int [19, 20]

to find all terms in eq. (1). For the terms in the first line, as well as for λ_5 , one has to add the hermitian conjugates as well. All Yukawas are to be understood as $(3, 3)$ matrices in generation space.

Note, that for $\lambda_5 \rightarrow 0$ lepton number is restored in the model. In this limit also neutrino masses vanish, so it is not allowed phenomenologically. However, since $\lambda_5 \rightarrow 0$ corresponds to a symmetry (lepton number conservation), small values of λ_5 are technically natural in the sense of t'Hooft. We also point out the interaction proportional to h_{ee} : This Yukawa coupling does not appear in the diagram fig. (1). However, all decays of our exotic particles must contain this coupling, we therefore call it loosely the “exit”, since for $\forall (h_{ee})_{ij} \equiv 0$ the lightest of the loop particles would be stable. Again, this limit is not allowed phenomenologically.

After electro-weak symmetry breaking, the doubly charged components in S_1 and S_3 mix. At tree-level their mass matrix is given by:

$$M_{2+}^2 = \begin{pmatrix} m_{S_1}^2 - \frac{1}{2}\lambda_2 v^2 & \frac{1}{2}\lambda_5 v^2 \\ \frac{1}{2}\lambda_5 v^2 & m_{S_3}^2 - \frac{1}{2}\lambda_{3a} v^2 \end{pmatrix}. \quad (2)$$

This matrix can easily be diagonalized analytically. The mixing angle can be expressed as:

$$\tan 2\theta = \frac{\lambda_5 v^2}{(m_{S_3}^2 - m_{S_1}^2) - \frac{1}{2}(\lambda_{3a} - \lambda_2)v^2}. \quad (3)$$

We will call the mass eigenstates H_i^{2+} , with $i = 1, 2$, the symbol S is reserved for gauge states. Also the mass eigenstates H^{3+} and H^{4+} receive a contribution to their mass proportional to the Higgs vev:

$$\begin{aligned} m_{4+}^2 &= m_{S_3}^2 - \frac{1}{2}(\lambda_{3a} + \lambda_{3b})v^2, \\ m_{3+}^2 &= m_{S_3}^2 - \left(\frac{1}{2}\lambda_{3a} + \frac{1}{4}\lambda_{3b}\right)v^2. \end{aligned} \quad (4)$$

As eq. (4) shows, $m_{4+}^2 < m_{3+}^2$ if $\lambda_{3b} > 0$. Note that the signs of the λ_i can be chosen freely. For values of m_{S_3} much larger than v and/or for $\lambda_i \ll 1$ one expects that the states H^{3+} , H^{4+} and one of the H^{2+} will be nearly degenerate.

The neutrino mass matrix in this model can be written as:

$$m_\nu = \mathcal{F} \times (h_{\bar{F}}^T \mathcal{M} h_F + h_F^T \mathcal{M} h_{\bar{F}}) \quad (5)$$

Here, $\mathcal{F} \simeq 1/(32\pi^2) \sin(2\theta)$ and \mathcal{M} is a $(3, 3)$ matrix with diagonal entries given by:

$$\mathcal{M}_{ii} = m_{F_i} \Delta B_0(x_1^2, x_2^2), \quad (6)$$

where $x_{1,2} = m_{2+, (1,2)}/m_{F_i}$ and

$$\Delta B(x, y) = x \frac{\log(x)}{(x-1)} - y \frac{\log(y)}{(y-1)}. \quad (7)$$

As eq.(5) shows, the neutrino masses depend on the product of two Yukawa couplings, which in principle can be different. A complete fit to neutrino data therefore requires the use of the formulas presented in [21, 22], which are a generalization of the well-known Casas-Ibarra parametrization [23].

Next we present some approximation formulas for the scalar decay widths, since these will be useful to understand our numerical results for the decay lengths, shown in the next section. In these estimates, we always neglect final state masses for simplicity. Assuming $\theta \ll 1$,³ the mass eigenstates $H_{1,2}^{2+}$ can be identified with the gauge eigenstates to a good approximation. The two-body decay widths, neglecting lepton masses, are:

$$\Gamma(H_i^{2+}) = 2c_{2+} \frac{|h_{ee}|^2}{8\pi} m_{H_i^{2+}}, \quad (8)$$

with $c_{2+} \simeq \cos\theta$ ($\sin\theta$), if the H_i^{2+} state is mostly singlet (triplet). Unless $|h_{ee}|$ is extremely tiny, one expects that the 2-body decay of the mostly singlet state, S_1^{2+} , is too fast to give a measurable decay length.

³ This corresponds to $\lambda_5 < 1$, compare to eq. (3).

For the decays of the states H^{3+} and H^{4+} , the decay widths depend mainly on the mass ordering of the exotic states in our model. If any $m_{F_i} < m_{H^{n+}}$ the decays of the scalars are 2-body and, again, one expects them to be too fast to leave experimentally interesting decay lengths. Similarly, if $m_{S_1} < m_{S_3}$, the multi-charged scalars will promptly decay to $H_1^{2+} \simeq S_1^{2+}$ plus W -boson(s). However, the situation is very different if $m_{S_3} < m_{S_1}, m_{F_1}$. Let us estimate the widths in this phenomenologically more interesting case.

Consider first H^{3+} . For this state we need to take into account two possible final states. The simpler one is the 3-body decay $H^{3+} \rightarrow W^+ l_\alpha^+ l_\beta^+$. One can derive the simple estimate:

$$\Gamma(H^{3+} \rightarrow W^+ l_\alpha^+ l_\beta^+) \simeq \frac{g_2^2}{2} \frac{|(h_{ee})_{\alpha\beta}|^2 \sin^2 \theta}{f(3)} \frac{(m_{H^{3+}}^2 - m_W^2)^{7/2}}{m_{H_1^{2+}}^4 m_W^2} \quad (9)$$

Note the factor $1/m_W^2$, which is due to the massive gauge boson in the final state. The term $f(3)$ corresponds to the 3-body phase space factor for massless particles:

$$f(n) = 4(4\pi)^{(2n-3)}(n-1)!(n-2)! \quad (10)$$

Equation (9) represents a rough estimate for the true value of the width in the case $m_{S_1}^2 \gg m_{S_3}^2$ and $m_{H^{3+}} \gg m_W$.

The second important decay mode of H^{3+} is the 4-body decay: $H^{3+} \rightarrow l_\alpha^+ l_\beta^+ l_\gamma^+ \nu_\delta$. This decay proceeds via diagrams involving the exotic fermions F_k^{2+} and F_k^{3+} , such as, for example: $H^{3+} \rightarrow l_\gamma^+ (F_k^{2+})^* \rightarrow l_\gamma^+ \nu_\delta (H_i^{2+})^* \rightarrow l_\alpha^+ l_\beta^+ l_\gamma^+ \nu_\delta$. In principle, the width contains a double sum: Summing over the different charge states F_k^{2+} and F_k^{3+} , as well as over the generation k . For the latter, we define an effective reduced coupling:

$$|\sum_k (\frac{h_F^{\gamma k} h_{\bar{F}}^{\delta k} + h_F^{\delta k} h_{\bar{F}}^{\gamma k}}{m_{F_k}})| \equiv |\langle \frac{h_{F\bar{F}}^{\gamma\delta}}{m_F} \rangle| \quad (11)$$

Note that in case that all $m_{F_k} \equiv m_F$, the effective $\langle m_F \rangle$ simply reduces to m_F and can be taken out from the sum. With eq. (11), the 4-body decay width can be estimated to be very roughly:

$$\Gamma(H^{3+} \rightarrow l_\alpha^+ l_\beta^+ l_\gamma^+ \nu_\delta) \simeq \frac{c_3}{f(4)} |\langle \frac{h_{F\bar{F}}^{\gamma\delta}}{m_F} \rangle|^2 \frac{|(h_{ee})_{\alpha\beta}|^2}{m_{H_2^{2+}}^4} m_{H^{3+}}^7, \quad (12)$$

with⁴ $c_3 \sim (1/4)$. Note that, there is a contribution to 4-body final states with $\gamma = \delta$ from a diagram with $H^{3+} \rightarrow (W^+)^* l_\alpha^+ l_\beta^+ \rightarrow l_\alpha^+ l_\beta^+ l_\gamma^+ \nu_\gamma$. This diagram can be estimated from eq. (9), but replacing $f(3) \rightarrow f(4)$ and multiplying the width by $\text{Br}(W \rightarrow l + \nu)$. The two diagrams can interfere, thus the approximate expressions become unreliable if both diagrams give numerical values of the same order of magnitude.

If $m_{S_3} < m_{S_1}$ and $m_{S_3} < m_{F_1}$, H^{4+} has only 4-body decays. There are two different final states to consider: $H^{4+} \rightarrow l_\alpha^+ l_\beta^+ l_\gamma^+ l_\delta^+$ and $H^{4+} \rightarrow l_\alpha^+ l_\beta^+ W^+ W^+$. The decay to charged leptons proceeds through similar diagrams as discussed for $H^{3+} \rightarrow l_\alpha^+ l_\beta^+ l_\gamma^+ \nu_\delta$ above, see also fig. (2). The partial width is therefore estimated as:

$$\Gamma(H^{4+} \rightarrow l_\alpha^+ l_\beta^+ l_\gamma^+ l_\delta^+) \simeq \frac{c_4}{f(4)} |\langle \frac{h_{F\bar{F}}^{\gamma\delta}}{m_F} \rangle|^2 \frac{|(h_{ee})_{\alpha\beta}|^2}{m_{H_2^{2+}}^4} m_{H^{4+}}^7, \quad (13)$$

with $c_4 \sim (1/4)$, again simply fitted to the numerical result.

The decay $H^{4+} \rightarrow l_\alpha^+ l_\beta^+ W^+ W^+$ is caused by two different kind of Feynman diagrams, see fig. (2). The vertex $HHWW \propto g_2^2$, while $HHW \propto g_2 \partial_\mu$. Assuming $H_2^{2+} \simeq S_1$ is much heavier than $H_1^{2+} \simeq S_3^{2+}$ and further simplifying $m_{H^{4+}} \simeq m_{H^{3+}} \simeq m_{H_1^{2+}}$, the middle diagram in fig. (2) is estimated to generate a width of the order of

$$\Gamma(H^{4+} \rightarrow W^+ W^+ l_\alpha^+ l_\beta^+) \sim \frac{1}{f(4)} \frac{(g_2^2 \sin \theta |(h_{ee})_{\alpha\beta}|)^2}{m_W^4} m_{H^{4+}}^5. \quad (14)$$

We stress that this approximation fails rather badly if $m_{H^{4+}} \simeq m_{H^{3+}} \simeq m_{H_1^{2+}}$ is not true.

⁴ We have estimated only the contribution from one diagram and adjusted the prefactor c_3 to fit the absolute value of the numerical output of Madgraph5 v2.3.3 [24], see the next section, since eq. (12) is used only to understand the parameter dependence of the width.

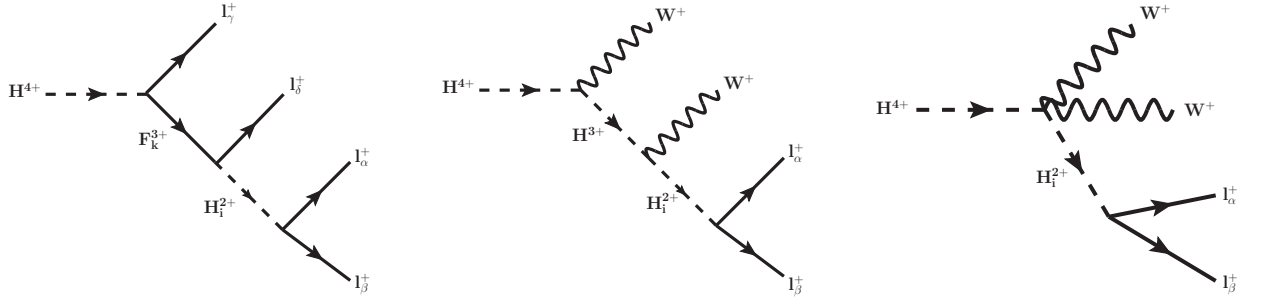


FIG. 2: Feynman diagrams for the decays $H^{4+} \rightarrow l_\gamma^+ l_\delta^+ l_\alpha^+ l_\beta^+$ and $H^{4+} \rightarrow W^+ W^+ l_\alpha^+ l_\beta^+$.

Finally, consider the case that one of the exotic fermionic states is the lightest new particle: $m_{F_1} < m_{S_1}, m_{S_3}$. Electroweak radiative corrections generate a small mass splitting between the F^{3+} and F^{2+} members of the $F_{1,2,5/2}$ multiplet(s). Using the results of [25, 26], we estimate $\Delta M = m_{F^{3+}} - m_{F^{2+}} \sim 1.6$ GeV for $m_F \gtrsim 500$ GeV. The F^{3+} then has a 2-body decay mode $F^{3+} \rightarrow F^{2+} + \pi^+$, with a width of order $(2-3)$ meV, again using the formulas of [25, 26]. Thus, F^{3+} decays can not be long-lived.

For F^{2+} , on the other hand, the main decay channel is to 3 standard model leptons. This width is estimated as:

$$\Gamma(F_1^{2+} \rightarrow l_\alpha^+ l_\beta^+ \nu_\delta) \simeq \frac{|(h_F)_{\delta 1} (h_{ee})_{\alpha\beta}|^2}{512\pi^3} \frac{m_{F_1^{2+}}^5}{m_{S_1}^4}. \quad (15)$$

We now turn to a discussion of the numerical results.

III. NUMERICAL RESULTS

We have implemented the model discussed in section II in SARAH [27, 28]. SARAH allows to automatically generate SPheno routines [29, 30] with which one can do a numerical evaluation of mass spectra, mixing matrices, 2-body and fermionic 3-body decays. SARAH also generates model files for MadGraph [24, 31, 32]. We use MadGraph to numerically calculate the 3-body and 4-body decay widths of the exotic scalars, as well as production cross sections.

A. Decay lengths

In this section we will discuss numerical results for the decay lengths of the new particles in our model. Let us start by stressing again that the mass ordering of the scalars, H_i^{2+} , H^{3+} and H^{4+} , and fermions, F_i^{2+} , is not fixed. If $H_1^{2+} \simeq S_1^{2+}$ is the lightest of the exotic particles, all heavier particles will decay fast to $H_1^{2+} + X$, where X stands symbolically for any other particle(s), and all decays in the model are most likely prompt. We will therefore discuss in detail only the case when the mostly S_1^{2+} state is heavier than the other particles.

As eqs (2) and (4) show, for moderate values of m_{S_3} and large values of $\lambda_{3a,3b}$, sizeable splittings among the members of the triplet are possible. Once the mass splitting is bigger than the mass of the W , decays such as $H^{4+} \rightarrow H^{3+} + W^+$ will dominate the total width. These decays are not suppressed by small neutrino masses and are therefore fast. We thus implicitly assume in the following discussion that the particle under consideration is the lightest member of the triplet.

Before showing the numerical results, let us briefly discuss how to fit the experimentally observed neutrino masses in our model. Consider the neutrino mass matrix, eq. (5). In our numerical calculations we use formulas from [21, 22] to parametrize the Yukawa couplings as:

$$h_F = \frac{1}{\sqrt{2\mathcal{F}}} \mathcal{M}^{-1/2} W T \bar{D} \sqrt{m} U_\nu^\dagger, \quad (16)$$

$$h_{\bar{F}} = \frac{1}{\sqrt{2\mathcal{F}}} \mathcal{M}^{-1/2} W^* B \bar{D} \sqrt{m} U_\nu^\dagger.$$

Here, W and T are a unitary and an upper-triangular matrix, while $B = (T^T)^{-1}(\mathbb{I}_3 + K)$, with K an anti-symmetric square matrix [22]. $\bar{D} \sqrt{m}$ and U_ν^\dagger are the square roots of the light neutrino mass eigenvalues and the neutrino mixing

matrix, respectively. \mathcal{M} and \mathcal{F} are defined in eq. (5). Eq. (16) is the generalization of the well-known Casas-Ibarra parametrization [23] for the case of two independent Yukawa matrices. Note, that if we choose the particular simple limit of $K = 0$ and T diagonal (\hat{T}), the three vectors in h_F and $h_{\bar{F}}$ are fixed only up to a constant T_{ii} each: $h_F \rightarrow \hat{T} h_F$ with $h_{\bar{F}} \rightarrow \hat{T}^{-1} h_{\bar{F}}$ leaves the neutrino masses unchanged. Essentially, eq. (16) fixes a relation between the measured neutrino data, see for example [33], and the Yukawa couplings h_F and $h_{\bar{F}}$. Once Δm_{Atm}^2 , Δm_{\odot}^2 and the neutrino mixing angles are fixed from data, for any set of scalar and fermion masses, plus a chosen neutrino mass scale m_{ν_1} , h_F and $h_{\bar{F}}$ can be fixed as function of λ_5 .

A simple estimate for the neutrino mass can be obtained, assuming all heavy masses approximately equal to some scale Λ and $\lambda_5 \ll 1$. Roughly,

$$m_\nu \simeq 0.05 \left(\frac{\lambda_5}{10^{-6}} \right) \left(\frac{h_F}{10^{-2}} \right) \left(\frac{h_{\bar{F}}}{10^{-2}} \right) \left(\frac{1 \text{ TeV}}{\Lambda} \right) \text{ eV}. \quad (17)$$

Neutrino masses only require that the product of $\lambda_5 h_F h_{\bar{F}}$ is small, but do not fix the ratios of these parameters. Recall, $\sin 2\theta \propto \lambda_5$. We do not use eq. (17) in our numerical studies. It serves only to show the order of magnitude of the parameters, necessary to explain neutrino data.

Let us discuss now scalar decays. Experimentally, the most interesting decays are those of the H^{4+} . As discussed in section II, for H^{4+} we have to consider two final states: $H^{4+} \rightarrow l_\gamma^+ l_\delta^+ l_\alpha^+ l_\beta^+$ and $H^{4+} \rightarrow W^+ W^+ l_\alpha^+ l_\beta^+$. Pair production of $H^{4+} H^{4-}$, see section III B, will then lead to final states $(4l^+)(4l^-)$, $(2l^+ 2l^- + 2W^+ 2W^-)$ and $(4l^\pm)(2l^\mp) + 2W^\mp$. The last one of these is the most interesting one, since it allows to demonstrate the existence of LNV experimentally, for those events where both the W s decay hadronically.⁵

The final state $6l + 2W$ can occur with measurable rates only if $\Gamma(H^{4+} \rightarrow 4l^+) \sim \Gamma(H^{4+} \rightarrow 2l^+ 2W^+)$, since otherwise the branching ratio into either the $4l$ or $2l + 2W$ final state is likely to be too small to be observed. Recall from the discussion in the previous section, $\Gamma(H^{4+} \rightarrow 4l^+) \propto h_F h_{\bar{F}}$, while $\Gamma(H^{4+} \rightarrow 2l^+ + 2W^+) \propto \lambda_5$.

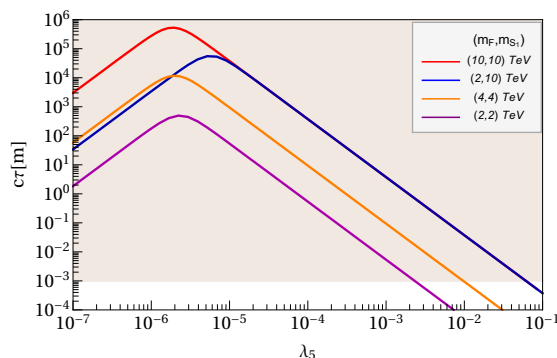


FIG. 3: Decay length of H^{4+} as a function of λ_5 , for fixed choices of other parameters. The lightest neutrino mass was fixed to $m_{\nu_1} = 1 \text{ meV}$, see also the text.

In fig. (3) we show $c\tau$ for the decay of H^{4+} as a function of λ_5 for three sets of arbitrary masses, but other parameters fixed. The red/blue/orange/purple curves correspond to (m_F, m_{S_1}) equal to $(10, 10)/(2, 10)/(4, 4)/(2, 2)$ TeV, respectively. We have also fixed $m_{H^{4+}} = 1 \text{ TeV}$ and $(h_{ee})_{11} = 0.1$ ($\forall (h_{ee})_{ij} = 0$).⁶ The Yukawa couplings h_F and $h_{\bar{F}}$ are calculated in each point using eq. (16) to explain the best fit point of neutrino oscillation data. The plot corresponds to $m_{\nu_1} = 10^{-3} \text{ eV}$ (and normal hierarchy). There is only a moderate dependence of the decay lengths on the choice of the lightest neutrino mass. As the plot shows, the decays of the H^{4+} are slow and long charged tracks are to be expected in large parts of the parameter space, unless $\lambda_5 \rightarrow 1$ or $\lambda_5 \rightarrow 0$.

The plots in fig. (3) show that $c\tau$ is maximized for intermediate values of λ_5 . This is easily understood from our neutrino fit. Consider eq. (17). Keeping the neutrino mass fixed, lower values of λ_5 require an increase of $h_F h_{\bar{F}}$. This increases $\Gamma(H^{4+} \rightarrow 4l^+)$. Equally, large λ_5 increases $\Gamma(H^{4+} \rightarrow 2l^+ + 2W^+)$. The maximal $c\tau$ therefore corresponds to the point where both partial widths are equal, and minimized in absolute value. In other words, the possibility to observe LNV experimentally is largest for the points with the largest $c\tau$.

⁵ Since $\text{Br}(W \rightarrow \text{hadrons}) \simeq 0.67$ [34], this corresponds to about half of all events. The remaining events contain leptonic decays of the W , i.e. missing energy in the final state.

⁶ This choice was only motivated to speed up the numerical calculations. The total width always scale perfectly with $|h_{ee}| = \sum \sqrt{(h_{ee})_{ij}^2}$.

One word of caution. One should not take the decay lengths in fig. (3) as fixed predictions, since (h_{ee}) is not fixed by neutrino data. Since all decay widths of H^{4+} are proportional to $(h_{ee})^2$ both, larger and smaller, $c\tau$ than the ones shown in (3) are allowed from the model. Note, however, that (h_{ee}) can not be arbitrarily small, since big bang nucleosynthesis disfavors particles with life-times larger than $\mathcal{O}(0.1 - 1)$ s [35–37].

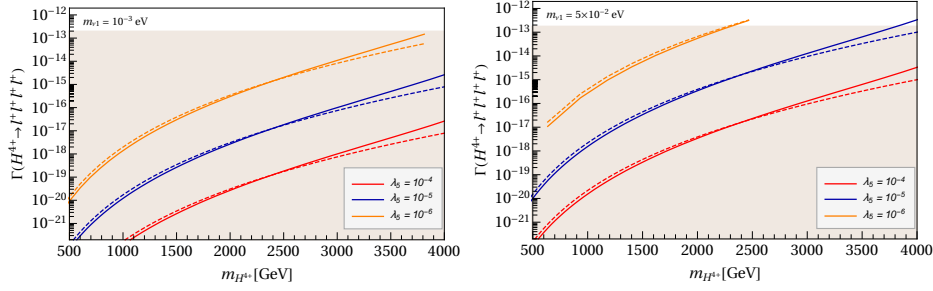


FIG. 4: Decay width of $H^{4+} \rightarrow 4l$ as a function of $m_{H^{4+}}$, for fixed choices of other parameters. $(h_{ee})_{11} = 1$, $m_F = 5$ TeV, $m_{S_1} = 5$ TeV and $\lambda_5 = 10^{-4}, 10^{-5}, 10^{-6}$ (red, blue, orange). h_{FFB} chosen to fit the neutrino masses. Solid and dashed lines correspond to numerical calculations and analytical estimations respectively.

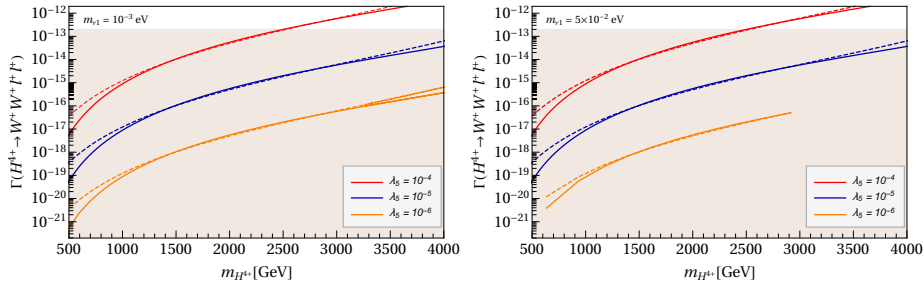


FIG. 5: Partial decay width of $H^{4+} \rightarrow 2W2l$ as a function of λ_5 , for fixed choices of other parameters. Parameters as in fig. (4).

Figs (4) and (5) show the partial widths for H^{4+} for the final states $H^{4+} \rightarrow 4l$ and $H^{4+} \rightarrow 2W2l$, respectively, as a function of $m_{H^{4+}}$ for fixed choice of other parameters. The plots serve only to demonstrate the strong dependence of the widths on $m_{H^{4+}}$. However, measurably small widths can occur even for the largest masses shown. Note, that the plots show partial widths and not decay lengths. The plots also demonstrate that there is some dependence of the widths on the absolute scale of neutrino mass. Since the lightest neutrino mass is currently unknown (only upper limits exist), larger lengths than shown in the plot are possible. (Again, the same is true for h_{ee} , see discussion above.)

We now turn to the discussion of the decay lengths for H^{3+} . Fig. (6) shows $c\tau$ for H^{3+} as a function of λ_5 for the same parameters as used in fig. (3). In the part of parameter space where the 4-body final state $H^{3+} \rightarrow 3l + \nu$ dominates, the decay lengths of H^{3+} are similar to those of H^{4+} , whereas for larger values of λ_5 , when $H^{3+} \rightarrow W + 2l$ dominates, the lengths of H^{3+} are expected to be around two orders of magnitude smaller than those for H^{4+} . The overall dependence of parameters is, however, very similar to those discussed for H^{4+} . Note, however, that the LNV final state for $H^{3+}H^{3-}$ pair production involves always at least one neutrino, and thus can not be used to demonstrate LNV experimentally.

Finally, let us briefly discuss the decays $H_1^{2+} \rightarrow l_\alpha^+ l_\beta^+$. Since these are 2-body decays, the $c\tau$ of H_1^{2+} is always shorter than those found for H^{3+} and H^{4+} . Nevertheless, for the $H_1^{2+} \simeq S_3^{2+}$ state, one can estimate

$$c\tau(H_1^{2+}) \simeq 1 \left(\frac{0.1}{|h_{ee}|} \right)^2 \left(\frac{10^{-5}}{|\lambda_5|} \right)^2 \left(\frac{1 \text{ TeV}}{m_{H_1^{2+}}} \right) \left(\frac{m_{S_1}}{2 \text{ TeV}} \right)^4 \text{ cm.} \quad (18)$$

Before closing this subsection, we mention that one expects that the fermion decays are rather fast. Let us assume for this estimate that one of the fermions is the lightest exotic particle. One then can make a rough guess that

$$c\tau(F_1) \simeq 5 \times 10^{-8} \left(\frac{0.1}{|h_{ee}|} \right)^2 \left(\frac{10^{-2}}{|h_F|} \right)^2 \left(\frac{1 \text{ TeV}}{m_{F_1}} \right) \left(\frac{m_{S_1}}{2 \text{ TeV}} \right)^4 \text{ m.} \quad (19)$$

Thus, unless $|h_F|$ is very small or m_{S_1} very large, one expects that the exotic fermions of this model decay promptly.

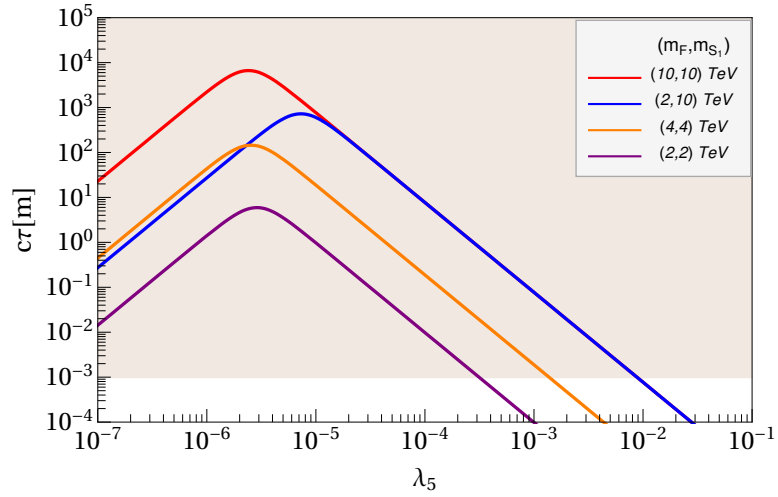


FIG. 6: Decay length of H^{3+} as a function of λ_5 , for fixed choices of other parameters. All other parameters as in fig. (3).

B. Cross sections, current limits and future expectations

In this subsection we will show the results for pair-production cross sections for the exotic scalars of our neutrino mass model. We will then discuss various LHC searches, from which limits on the parameter space of the model can be currently derived. We will use these limits to estimate the discovery prospects for the high-luminosity LHC, i.e. for the expected future $\mathcal{L} = 3/\text{ab}$ of statistics. We also mention briefly the expectations for a hypothetical 100 TeV proton-proton collider.

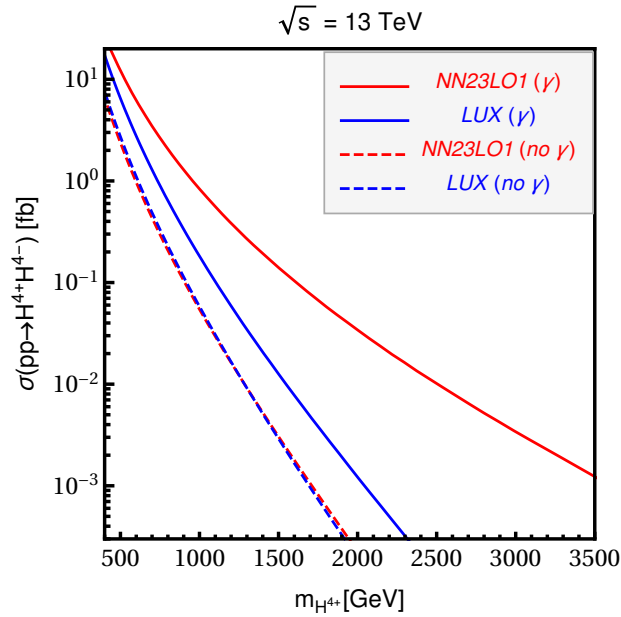


FIG. 7: Pair production cross sections for $H^{4+}H^{4-}$ at the LHC for $\sqrt{s} = 13$ TeV using different PDFs. For a discussion see text.

Pair production of multiply charged particles is dominated by photon-photon fusion diagrams, which are very important in particular at large scalar masses, despite the tiny parton density of the photon inside the proton. This has been discussed recently for example in [38]. MadGraph [32] uses NNPDF23LO [39] as the standard choice for the parton distribution function (PDF). However, as discussed in the context of a cross section calculation [40] for the “BNT” neutrino mass model [41], large uncertainties in the photon density in NNPDF23LO lead to large uncertainties in predicted cross sections. On the other hand, Manohar et al. [42, 43] have discussed a model-

independent determination of the photon PDF inside the proton, leading to much smaller errors in the determination of the photon density within the proton. The resulting LUXqed17_plus_PDF4LHC15_nnlo_100 combines QCD partons from PDF4LHC15 [44] with the LUXqed calculation of the photon density.

We have therefore calculated cross sections for pair production of $H^{4+}H^{4-}$ for both, NNPDF23LO and LUXqed PDFs. Fig. (7) shows the results for NNPDF23LO (in red) and LUXqed17 (blue) including the photon content (full lines) and without photon-photon fusion diagrams (dashed lines). Putting the photon density in the proton artificially to zero, NNPDF23LO and LUXqed17 lead to very similar results, as can be seen from the figure. On the other hand, the figure shows that NNPDF23LO leads to significantly larger cross sections than LUXqed17, once the photon-fusion diagrams are included in the calculation. The plot also demonstrates that even for the LUXqed17, with much smaller photon densities, photon-photon fusion diagrams dominate the cross section, especially at large masses.

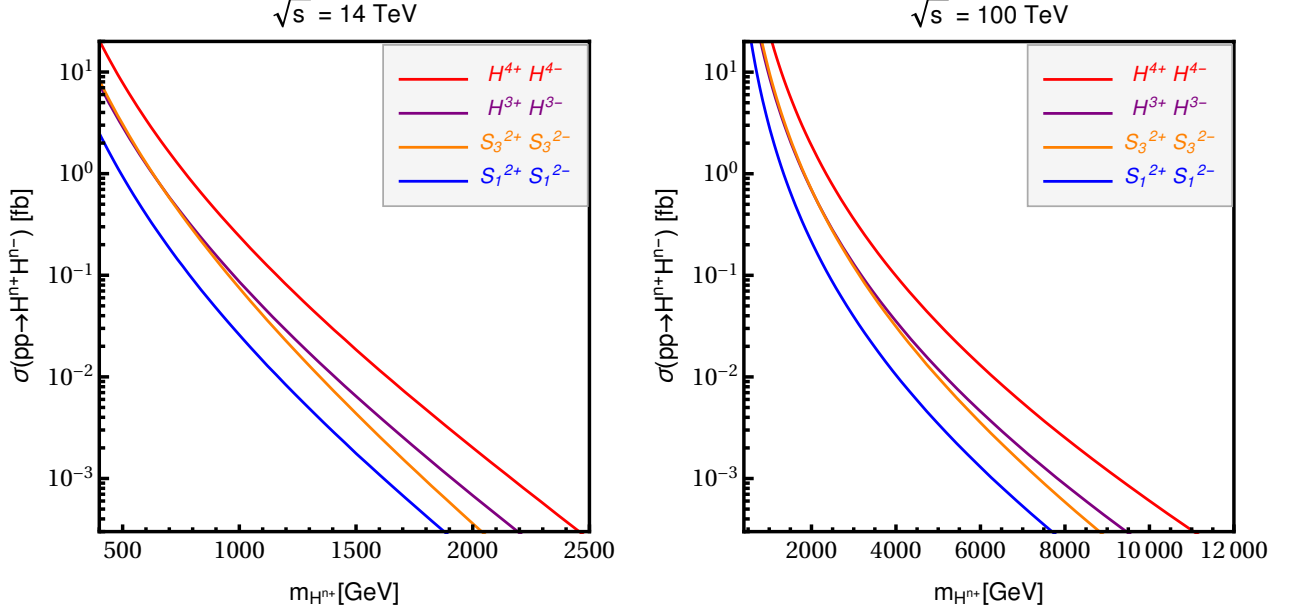


FIG. 8: Pair production cross sections for the different charged scalars in our model. The calculation was done with LUXqed17_plus_PDF4LHC15_nnlo_100 [42, 43] and includes photon-photon fusion diagrams. To the left $\sqrt{s} = 14$ TeV, to the right $\sqrt{s} = 100$ TeV.

Given the importance of photon-fusion diagrams in our calculation and considering that the LUXqed PDFs have been calculated specifically to reduce the error in the photon density [42, 43], we will base our discussion on the LHC sensitivity on cross section calculations using the LUXqed17_plus_PDF4LHC15_nnlo_100 PDFs. Fig. (8) shows cross sections for the four different charged scalars as a function of their mass. The left of the figure shows the results for $\sqrt{s} = 14$ TeV, while the plot on the right is for pp-collisions at $\sqrt{s} = 100$ TeV. We mention that, similar to fig. (7), the cross sections calculated with the NNPDF23LO PDF are much larger than those shown in the figure. However, we will not use the NNPDF23LO PDF results in the following and thus, do not show the corresponding plots.

We now turn to a discussion of LHC searches. While none of the existing searches of ATLAS and CMS covers exactly the multi-lepton signals we are interested in, several of the “exotics” searches can be used to put limits on the parameter space of our model. We can roughly divide these searches into three categories: (i) quasi-stable particles, i.e. $c\tau$ of the order or larger than typical detector sizes; (ii) finite $c\tau$, say $c\tau \sim \mathcal{O}(10^{-3} - 1)$ m. And, finally, (iii) prompt decays.

ATLAS has searched for stable (or *quasi-stable*) multi-charged particles (“MCPs”) in run-II with $\sqrt{s} = 13$ TeV and $\mathcal{L} = 36.1/\text{fb}$ of statistics [45].⁷ In this search [45] the MCPs are assumed to live long enough to traverse the entire ATLAS detector without decaying, and thus the analysis exploits their muon-like signature. The search is based on the anomalously large ionization loss of particles with $|q| = ze$ and $z \geq 2$ that are long-lived enough to reach (and traverse) the muon spectrometer. This implies that the maximum efficiency of this search is reached for $c\tau$ larger or

⁷ Also CMS searched for long-lived charged particles [46]. However, the CMS publication is based on only $\mathcal{L} = 2.6/\text{fb}$ and thus currently is not competitive with the ATLAS limits discussed here.

equal roughly order $c\tau \sim 10$ m. There is a trigger on particles with $\beta > 0.6$, due to a timing window. This requirement reduces the trigger efficiency for the largest masses and charges. ATLAS therefore applied a second possible trigger in this search based on E_T^{miss} , with $E_T^{miss} > 70, 90$ and 110 GeV, for different data subsets. This second trigger, however, is responsible only for about 20 % of the overall signal events.

This search does not cover our multi-lepton signal, and in particular can not establish LNV. Nevertheless, this search can be recast to give an estimate of the LHC sensitivity for the model parameter space, where $c\tau \sim 10$ m or larger. The ATLAS simulation shows that this search is essentially background free, with an estimated number of background events less than $0.26 [5.1 \times 10^{-2}]$ for $z = 2 [z > 2]$. ATLAS then shows, see fig. (8) of [45], upper limits on the production cross section as function of mass for different choices of z . Experimental limits are in the range of $(0.2 - 0.4)$ fb in the range of masses $(200 - 1400)$ GeV, for $z = (2 - 5)$. From our calculated cross sections we can then estimate lower limits on the scalar masses: $m_{H^{4+}} \gtrsim 980$ GeV, $m_{H^{3+}} \gtrsim 820$ GeV, $m_{H^{2+}} \gtrsim 800$ GeV (for a mostly triplet state) and $m_{H^{2+}} \gtrsim 660$ GeV (for a $SU(2)_L$ singlet state). We mention again that these limits apply only for particles with $c\tau$ larger than a few m.

We also want to stress the importance of the photon-fusion diagrams. The limit on $m_{H^{4+}}$, for example, would change to $m_{H^{4+}} \gtrsim 820$ GeV, excluding these diagrams from the calculation. Even more important is the correct choice of the PDF. Using NNPDF23LO one would have estimated an unrealistically large limit of $m_{H^{4+}} \gtrsim 1380$ GeV.

Since this search is background free, we can make estimates for future sensitivities by simply scaling existing limits with the expected luminosity gain. For $\mathcal{L} = 3/\text{ab}$, we obtain with this procedure $m_{H^{4+}} \gtrsim 2$ TeV, $m_{H^{3+}} \gtrsim 1.7$ TeV, $m_{H^{2+}} \gtrsim 1.6$ TeV (triplet) and $m_{H^{2+}} \gtrsim 1.4$ TeV (singlet). For completeness we mention the corresponding numbers for a $\sqrt{s} = 100$ TeV collider with $\mathcal{L} = 30/\text{ab}$: $m_{H^{4+}} \gtrsim 11.4$ TeV, $m_{H^{3+}} \gtrsim 10$ TeV, $m_{H^{2+}} \gtrsim 9$ TeV (triplet) and $m_{H^{2+}} \gtrsim 8$ TeV (singlet).

A search for decays of stopped exotic long-lived particles has been published by CMS [47]. The search is based on stopped particles decaying to hadronic final states in the calorimeter or to final states involving muons in the muon spectrometer. Statistics is $\mathcal{L} = 38.6/\text{fb}$ (39.0/fb) for calorimeter (MS) search. Cross-section limits assume specific final states, non of which is our multi-lepton signal. Thus, these limits do not apply directly to our model. However, we mention that the best limits are of the order of $(20 - 500)$ fb for a time window of $(10^{-6} - 10^5)$ sec and it can be expected that a search for the more complicated final states, as we are interested in, would give similar results. At least currently, however, these numbers are not competitive with the charged track search discussed above.

For $c\tau$ in the intermediate region, say ($c\tau = 1$ mm - 1 m), there is currently no search in ATLAS or CMS that can be directly converted into limits on the parameters of our model. In this $c\tau$ region, the model predicts as signal tracks with anomalously large ionization loss, corresponding to the multiple electric charges, with multiple leptons (with or without jets from the gauge boson decays) at the end of the tracks.

CMS has searched for events with oppositely charged, displaced electrons and muons at 8 TeV [48] (with 19.7 fb^{-1}) and 13 TeV [49] (with 2.6 fb^{-1}). Also ATLAS has looked for displaced vertices made from pairs of leptons decaying inside the tracker at 8 TeV (with 20.3 fb^{-1}) [50]. Searches for displaced lepton pairs or displaced secondary vertices (where the leptons are associated back to the same vertex) can be applied to derive limits on S^{2+} . The search by CMS [49] gives currently the strongest limit. Their search was motivated by a supersymmetric model and their lower limit on the scalar top mass of $m_{\tilde{t}_1} \gtrsim 870$ GeV corresponds to an upper limit of roughly $\sigma \times Br \simeq 10$ fb. Assuming that a same-sign lepton search would have a similar limit,⁸ rough estimates of $m_{H^{2+}} \gtrsim 370$ GeV (270 GeV) for mostly triplet (singlet) for a branching ratio to electron-muon final state equal to one can be estimated from this. Again, the limit is not very strong since the statistics is based on only $2.6/\text{fb}$.

Both, CMS [51] and ATLAS [52] have searched for “disappearing tracks”. These events are defined to contain an isolated (charged) short track with⁹, (i) little or no energy in associated calorimeter deposits, and (ii) no associated hits in SCT and muon detectors. In addition, events are selected by requiring (iii) large E_{miss} in the event, which is ensured by the presence of a high p_T ISR jet. While a charged track search would cover the intermediate $c\tau$ region of our multi-lepton signature in principle, the requirements (i)-(ii)-(iii) make it difficult that these searches are used as constraint. Nevertheless, disappearing track searches could have some sensitivity to “kinked track” signals, as shown for example in [53]. Specially stronger limits could be obtained with some trigger modifications, by cutting directly on the measured track momentum [54]. This encourages the experimental collaborations to study extensions and/or modifications of existing disappearing track search strategies. We note that these searches [51, 52] are actually not background free. Adding (displaced) charged leptons (and jets) to the track search should actually yield lower backgrounds and we expect that limits from a dedicated search would be close to background free and thus yield

⁸ Same-sign di-lepton searches usually have less background than opposite-sign di-leptons. This assumption should therefore be conservative.

⁹ A short track or “tracklet” requires no associated hits beyond the pixel layers as a “disappearance condition”.

much stronger limits than those derived in [51, 52].

Searches for multitrack displaced vertices [50, 55] could, in principle, also be sensitive to the model parameters, when the charged H^{n+} decay within the inner tracker of ATLAS and/or CMS (or within roughly $c\tau = 4 - 300$ [mm]). Ref. [55], based on 32.8/fb, gives the strongest upper limit at $c\tau = 3$ cm of 0.15 fb. This limit, however, is a combination of different final state searches, at least one class of events including a high E_{miss} cut. We therefore can not directly convert this limit into a lower limit on the scalar masses. However, it was shown that displaced vertex searches can be reinterpreted in the context of neutrino mass models by requiring a lepton trigger [56, 57]. The ATLAS experiment performed such search when two lepton-tracks are coming from the displaced vertex [58]. When no other associated prompt objects are available to trigger on, one can require the lepton to be explicitly associated to the displaced vertex [59].

For the parameter region of our model where the scalars decay promptly, various “seesaw-searches” can give limits on our model parameters. CMS has updated their seesaw type-III search in [18]. This paper is based on $\mathcal{L} = 137/\text{fb}$. The signal in this search is *at least three charged leptons plus missing energy*. These limits therefore can be converted into limits only for H^{3+} and for that part of parameter space where H^{4+} decays to the $2W2l$ final state (with the W ’s decaying leptonically). Limits are given unfortunately only for the “flavour-democratic” scenario, i.e. the decays of the heavy leptons (charged and neutral) are assumed to have equal branching ratios for e, μ and τ . Note that this limit is rather sensitive to this assumption. Recall, that in the earlier analysis of [60] limits in the range (390-930) GeV were found, when varying the branching ratios to the different charged lepton generations from zero to one. The upper limit depends on the assumed mass of the heavy state searched for and range from order 10 fb at 500 GeV, to as low as (2 – 3) fb for masses in the range 1 – 1.4 TeV. This does not yet give meaningful limits, but will be interesting to constrain our exotic scalars, once more statistics is accumulated.

Our H^{2+} ’s are also constrained by seesaw type-II searches, such as [61–63]. For decays dominantly to muon the limit is 0.87 TeV [61]. The search to WW final states [63] does not apply to our model. Note again, that these searches apply for prompt decays.

Finally, the MoEDAL [64] experiment currently running at the LHC is also sensitive to highly-ionising particles. Although designed to search for magnetic monopoles (see for instance [65]), it also has sensitivity to electrically-charged massive long-lived particles. Our states are potentially detectable in MoEDAL if they are produced with low velocities ($\beta < 0.2$) and travel at least a meter. These would complement the accessible region at ATLAS and CMS, usually targeting $\beta > 0.2$, as mentioned above.

In summary, limits on the scalars of our model can be derived from various existing searches. Background-free searches could be done for the parts of parameter space, where at least H^{4+} is long-lived enough to leave a charged track in the detector. None of the current searches, however, covers exactly the final states from H^{4+} decays. We can therefore give only rough estimates on the mass limits for our model at present.

IV. SUMMARY AND DISCUSSION

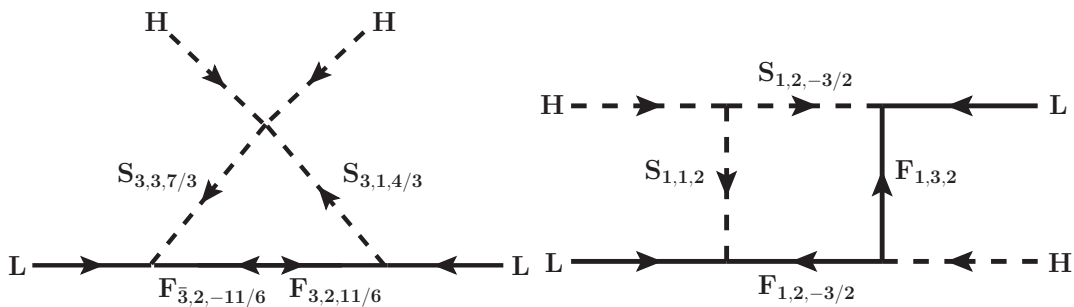


FIG. 9: Two more variants of $d = 5$ 1-loop models that lead to exotic LNV signals at the LHC. Left (model-II) a leptoquark variant, right (model-III) a variant based on a different one-loop neutrino mass topology. For a discussion see text.

We have discussed multi-lepton LNV final states at the LHC. We have shown in one concrete 1-loop neutrino mass model that multi-lepton signals can occur with experimentally interesting rates. Moreover, the smallness of the observed neutrino masses, together with the high multiplicity of the final states, lead to tiny decay widths of the multi-charged scalars, resulting in long charged tracks in large parts of the available parameter space. This kind of exotic signals would be virtually background-free at the LHC (or a hypothetically future 100 TeV pp -collider). Already

with existing data, interesting bounds can be derived and we have discussed how to recast several searches in terms of the mass parameters of our model.

Before closing, we would like to discuss that the particular example we studied in this paper is not the only (loop) model of neutrino mass that leads to these exotic multi-lepton signals. Many other variants following the same basic idea can be constructed. Two examples are shown in fig. (9).

Model-II, see the diagram on the left of fig. (9), is based on the same topology as our proto-type model. However, here the particles in the loop carry colour. The model has two different scalar leptoquark states plus an exotic coloured fermion. Similar to our proto-type model, the phenomenologically most interesting decays are those of the scalar electro-weak triplet. This multiplet contains a particle $S_3^{10/3+}$, which can decay either to $(3l^+) + j$ or $l^+ + (2W^+) + j$. The LNV final state from pair-produced $S_3^{10/3+}$ will then consist of $(3l^\pm)l^\mp(2W^\mp)(2j)$. Compared to the $6l + 2W$ signal of our proto-type model, one can thus have signals with more jets and fewer charged leptons.¹⁰ On the other hand, since the neutrino mass calculation for this model and the multiplicity of the final state is very similar to the ones discussed in this paper, one can expect the different states of the $S_{3,3,7/3}$ to be long-lived, again, if they are the lighter than $S_{3,1,4/3}$ and the exotic fermion. Cross sections for coloured particles are larger than for coloured singlets at the LHC, so one can expect even larger sensitivity in pp -colliders for such kind of model variants.

Model-III, see the diagram on the right of fig. (9), is a model variant based on a different 1-loop topology. We have chosen to show this example to demonstrate that models with multi-lepton final states can arise from any loop topology. In this model, the particle with the largest charge is a triply charged fermion. The LNV multi-lepton final state for pair production of this particle will be $(3l^\pm)l^\mp(2W^\mp)$, similar to model-II above, but with fewer jets. For multiply charged fermions, however, QED radiative corrections will always produce a small mass splitting between states with different electrical charges and thus one finds for a $F_{1,3,2}$ that roughly $m_{F^{3+}} - m_{F^{2+}} \sim 1.5$ GeV. The F^{3+} will then decay to $F^{2+} + \pi^+$, unsuppressed by the small neutrino masses and this puts an upper limit on the decay length of F^{3+} . In this model variant one therefore does not expect charged tracks with LNV signals at the end of the tracks.

Multi-lepton signals are not limited to $d = 5$ neutrino mass models. Rather, using higher-dimensional operators to generate neutrino masses, requires larger representations (with non-zero hypercharge). At $d = 7$ one finds at tree-level the ‘‘BNT’’ model [41]. This model uses a scalar $S_{1,4,3/2}$, which contains a triply charged scalar. The decays of (pairs of) the S^{3+} of this model can lead to the final state $(2l^\pm)W^\pm(3W^\mp)$, with only two leptons, but accompanied by many jets from the hadronic decays of the W . The decays of S^{3+} , however, are expected to be rather short [66]. For neutrino mass models at $d = 7$ and 1-loop, multi-lepton signals will actually be the norm and not the exception. This can be seen from the example models discussed in [67] and easily deduced from the list of all possible $d = 7$ 1-loop diagrams given in [68].

In summary, multi-lepton signals, as discussed in this paper, can arise in a variety of neutrino mass models. Since these high multiplicity final states should have very little background at the LHC, dedicated searches have strong discovery potential. On top of that, even less background is expected if the charged particles are long-lived. None of the existing searches is optimized for the signals we have discussed, but interesting limits can already be derived from recasting current data.

Acknowledgments

M. H. is supported by the Spanish grant FPA2017-85216-P (AEI/FEDER, UE) and PROMETEO/2018/165 (Generalitat Valenciana). G.C. acknowledges support from FONDECYT-Chile grant No. 3190051. J. C. H. is supported by Chile grant FONDECYT No. 1161463. G.C. and J. C. H. also acknowledge support from grant FONDECYT No. 1201673. C.A. is supported by FONDECYT-Chile grant No. 11180722 and ANID-Chile PIA/APOYO AFB 180002.

-
- [1] ATLAS collaboration, M. Aaboud et al., *Search for heavy Majorana or Dirac neutrinos and right-handed W gauge bosons in final states with two charged leptons and two jets at $\sqrt{s} = 13$ TeV with the ATLAS detector*, *JHEP* **01** (2019) 016, [1809.11105].
 - [2] CMS collaboration, A. M. Sirunyan et al., *Search for a heavy right-handed W boson and a heavy neutrino in events with two same-flavor leptons and two jets at $\sqrt{s} = 13$ TeV*, *JHEP* **05** (2018) 148, [1803.11116].
-

¹⁰ Leptonic decays of W add more leptons, but also missing energy to the observed final state.

- [3] W.-Y. Keung and G. Senjanovic, *Majorana Neutrinos and the Production of the Right-handed Charged Gauge Boson*, *Phys. Rev. Lett.* **50** (1983) 1427.
- [4] A. Zee, *A theory of lepton number violation, neutrino Majorana mass, and oscillation*, *Phys. Lett.* **B93** (1980) 389.
- [5] T. P. Cheng and L.-F. Li, *Neutrino masses, mixings and oscillations in $SU(2)_L \times U(1)$ models of electroweak interactions*, *Phys. Rev.* **D22** (1980) 2860.
- [6] A. Zee, *Quantum numbers of Majorana neutrino masses*, *Nucl. Phys.* **B264** (1986) 99–110.
- [7] K. S. Babu, *Model of “calculable” Majorana neutrino masses*, *Phys. Lett.* **B203** (1988) 132–136.
- [8] Y. Cai, J. Herrero-García, M. A. Schmidt, A. Vicente and R. R. Volkas, *From the trees to the forest: a review of radiative neutrino mass models*, *Front. in Phys.* **5** (2017) 63, [[1706.08524](#)].
- [9] F. Bonnet, M. Hirsch, T. Ota and W. Winter, *Systematic study of the $d=5$ Weinberg operator at one-loop order*, *JHEP* **07** (2012) 153, [[1204.5862](#)].
- [10] D. Aristizabal Sierra, A. Degee, L. Dorame and M. Hirsch, *Systematic classification of two-loop realizations of the Weinberg operator*, *JHEP* **03** (2015) 040, [[1411.7038](#)].
- [11] R. Cepedello, R. M. Fonseca and M. Hirsch, *Systematic classification of three-loop realizations of the Weinberg operator*, *JHEP* **10** (2018) 197, [[1807.00629](#)], [erratum: *JHEP*06,034(2019)].
- [12] E. Ma, *Verifiable radiative seesaw mechanism of neutrino mass and dark matter*, *Phys. Rev.* **D73** (2006) 077301, [[hep-ph/0601225](#)].
- [13] P. Minkowski, $\mu \rightarrow e\gamma$ at a Rate of One Out of 10^9 Muon Decays?, *Phys. Lett.* **67B** (1977) 421–428.
- [14] R. N. Mohapatra and G. Senjanovic, *Neutrino Mass and Spontaneous Parity Violation*, *Phys. Rev. Lett.* **44** (1980) 912, [[231\(1979\)](#)].
- [15] J. Schechter and J. W. F. Valle, *Neutrino Masses in $SU(2) \times U(1)$ Theories*, *Phys. Rev.* **D22** (1980) 2227.
- [16] CMS collaboration, A. M. Sirunyan et al., *Search for heavy Majorana neutrinos in same-sign dilepton channels in proton-proton collisions at $\sqrt{s} = 13$ TeV*, *JHEP* **01** (2019) 122, [[1806.10905](#)].
- [17] CMS collaboration, A. M. Sirunyan et al., *Search for heavy neutral leptons in events with three charged leptons in proton-proton collisions at $\sqrt{s} = 13$ TeV*, *Phys. Rev. Lett.* **120** (2018) 221801, [[1802.02965](#)].
- [18] CMS collaboration, A. M. Sirunyan et al., *Search for physics beyond the standard model in multilepton final states in proton-proton collisions at $\sqrt{s} = 13$ TeV*, [1911.04968](#).
- [19] R. M. Fonseca, *Calculating the renormalisation group equations of a SUSY model with Susyno*, *Comput. Phys. Commun.* **183** (2012) 2298–2306, [[1106.5016](#)].
- [20] R. M. Fonseca, *The Sym2Int program: going from symmetries to interactions*, *J. Phys. Conf. Ser.* **873** (2017) 012045, [[1703.05221](#)].
- [21] I. Cordero-Carrión, M. Hirsch and A. Vicente, *Master Majorana neutrino mass parametrization*, *Phys. Rev.* **D99** (2019) 075019, [[1812.03896](#)].
- [22] I. Cordero-Carrión, M. Hirsch and A. Vicente, *General parametrization of Majorana neutrino mass models*, [1912.08858](#).
- [23] J. A. Casas and A. Ibarra, *Oscillating neutrinos and $\mu \rightarrow e, \gamma$* , *Nucl. Phys.* **B618** (2001) 171–204, [[hep-ph/0103065](#)].
- [24] J. Alwall, M. Herquet, F. Maltoni, O. Mattelaer and T. Stelzer, *MadGraph 5 : Going Beyond*, *JHEP* **1106** (2011) 128, [[1106.0522](#)].
- [25] M. Cirelli, N. Fornengo and A. Strumia, *Minimal dark matter*, *Nucl. Phys.* **B753** (2006) 178–194, [[hep-ph/0512090](#)].
- [26] R. Franceschini, T. Hambye and A. Strumia, *Type-III see-saw at LHC*, *Phys. Rev.* **D78** (2008) 033002, [[0805.1613](#)].
- [27] F. Staub, *SARAH 3.2: Dirac Gauginos, UFO output, and more*, *Comput. Phys. Commun.* **184** (2013) 1792–1809, [[1207.0906](#)].
- [28] F. Staub, *SARAH 4 : A tool for (not only SUSY) model builders*, *Comput. Phys. Commun.* **185** (2014) 1773–1790, [[1309.7223](#)].
- [29] W. Porod, *SPheno, a program for calculating supersymmetric spectra, SUSY particle decays and SUSY particle production at e^+e^- colliders*, *Comput. Phys. Commun.* **153** (2003) 275–315, [[hep-ph/0301101](#)].
- [30] W. Porod and F. Staub, *SPheno 3.1: Extensions including flavour, CP-phases and models beyond the MSSM*, *Comput. Phys. Commun.* **183** (2012) 2458–2469, [[1104.1573](#)].
- [31] J. Alwall, P. Demin, S. de Visscher, R. Frederix, M. Herquet, F. Maltoni et al., *MadGraph/MadEvent v4: The New Web Generation*, *JHEP* **09** (2007) 028, [[0706.2334](#)].
- [32] J. Alwall, R. Frederix, S. Frixione, V. Hirschi, F. Maltoni, O. Mattelaer et al., *The automated computation of tree-level and next-to-leading order differential cross sections, and their matching to parton shower simulations*, *JHEP* **07** (2014) 079, [[1405.0301](#)].
- [33] P. F. de Salas, D. V. Forero, C. A. Ternes, M. Tortola and J. W. F. Valle, *Status of neutrino oscillations 2018: 3σ hint for normal mass ordering and improved CP sensitivity*, *Phys. Lett.* **B782** (2018) 633–640, [[1708.01186](#)].
- [34] PARTICLE DATA GROUP collaboration, M. Tanabashi et al., *Review of Particle Physics*, *Phys. Rev.* **D98** (2018) 030001.
- [35] PLANCK collaboration, N. Aghanim et al., *Planck 2018 results. VI. Cosmological parameters*, [1807.06209](#).
- [36] M. Kawasaki, K. Kohri and T. Moroi, *Big-Bang nucleosynthesis and hadronic decay of long-lived massive particles*, *Phys. Rev.* **D71** (2005) 083502, [[astro-ph/0408426](#)].
- [37] K. Jedamzik, *Big bang nucleosynthesis constraints on hadronically and electromagnetically decaying relic neutral particles*, *Phys. Rev.* **D74** (2006) 103509, [[hep-ph/0604251](#)].
- [38] K. Ghosh, S. Jana and S. Nandi, *Neutrino Mass Generation at TeV Scale and New Physics Signatures from Charged Higgs at the LHC for Photon Initiated Processes*, *JHEP* **03** (2018) 180, [[1705.01121](#)].
- [39] NNPDF collaboration, R. D. Ball, V. Bertone, S. Carrazza, L. Del Debbio, S. Forte, A. Guffanti et al., *Parton distributions*

- with QED corrections, *Nucl. Phys.* **B877** (2013) 290–320, [[1308.0598](#)].
- [40] T. Ghosh, S. Jana and S. Nandi, *Neutrino mass from Higgs quadruplet and multicharged Higgs searches at the LHC*, *Phys. Rev.* **D97** (2018) 115037, [[1802.09251](#)].
 - [41] K. S. Babu, S. Nandi and Z. Tavartkiladze, *New Mechanism for Neutrino Mass Generation and Triply Charged Higgs Bosons at the LHC*, *Phys. Rev.* **D80** (2009) 071702, [[0905.2710](#)].
 - [42] A. Manohar, P. Nason, G. P. Salam and G. Zanderighi, *How bright is the proton? A precise determination of the photon parton distribution function*, *Phys. Rev. Lett.* **117** (2016) 242002, [[1607.04266](#)].
 - [43] A. V. Manohar, P. Nason, G. P. Salam and G. Zanderighi, *The Photon Content of the Proton*, *JHEP* **12** (2017) 046, [[1708.01256](#)].
 - [44] J. Butterworth et al., *PDF4LHC recommendations for LHC Run II*, *J. Phys.* **G43** (2016) 023001, [[1510.03865](#)].
 - [45] ATLAS collaboration, M. Aaboud et al., *Search for heavy long-lived multicharged particles in proton-proton collisions at $\sqrt{s} = 13$ TeV using the ATLAS detector*, *Phys. Rev.* **D99** (2019) 052003, [[1812.03673](#)].
 - [46] CMS collaboration, V. Khachatryan et al., *Search for long-lived charged particles in proton-proton collisions at $\sqrt{s} = 13$ TeV*, *Phys. Rev.* **D94** (2016) 112004, [[1609.08382](#)].
 - [47] CMS collaboration, A. M. Sirunyan et al., *Search for decays of stopped exotic long-lived particles produced in proton-proton collisions at $\sqrt{s} = 13$ TeV*, *JHEP* **05** (2018) 127, [[1801.00359](#)].
 - [48] CMS collaboration, V. Khachatryan et al., *Search for Displaced Supersymmetry in events with an electron and a muon with large impact parameters*, *Phys. Rev. Lett.* **114** (2015) 061801, [[1409.4789](#)].
 - [49] CMS collaboration, *Search for displaced leptons in the e-mu channel*, [CMS-PAS-EXO-16-022](#).
 - [50] ATLAS collaboration, G. Aad et al., *Search for massive, long-lived particles using multitrack displaced vertices or displaced lepton pairs in pp collisions at $\sqrt{s} = 8$ TeV with the ATLAS detector*, *Phys. Rev.* **D92** (2015) 072004, [[1504.05162](#)].
 - [51] CMS collaboration, A. M. Sirunyan et al., *Search for disappearing tracks as a signature of new long-lived particles in proton-proton collisions at $\sqrt{s} = 13$ TeV*, *JHEP* **08** (2018) 016, [[1804.07321](#)].
 - [52] ATLAS collaboration, M. Aaboud et al., *Search for long-lived charginos based on a disappearing-track signature in pp collisions at $\sqrt{s} = 13$ TeV with the ATLAS detector*, *JHEP* **06** (2018) 022, [[1712.02118](#)].
 - [53] J. A. Evans and J. Shelton, *Long-Lived Staus and Displaced Leptons at the LHC*, *JHEP* **04** (2016) 056, [[1601.01326](#)].
 - [54] R. Mahbubani, P. Schwaller and J. Zurita, *Closing the window for compressed Dark Sectors with disappearing charged tracks*, *JHEP* **06** (2017) 119, [[1703.05327](#)], [Erratum: *JHEP*10,061(2017)].
 - [55] ATLAS collaboration, M. Aaboud et al., *Search for long-lived, massive particles in events with displaced vertices and missing transverse momentum in $\sqrt{s} = 13$ TeV pp collisions with the ATLAS detector*, *Phys. Rev.* **D97** (2018) 052012, [[1710.04901](#)].
 - [56] G. Cottin, J. C. Helo and M. Hirsch, *Searches for light sterile neutrinos with multitrack displaced vertices*, *Phys. Rev.* **D97** (2018) 055025, [[1801.02734](#)].
 - [57] G. Cottin, J. C. Helo and M. Hirsch, *Displaced vertices as probes of sterile neutrino mixing at the LHC*, *Phys. Rev.* **D98** (2018) 035012, [[1806.05191](#)].
 - [58] ATLAS collaboration, G. Aad et al., *Search for heavy neutral leptons in decays of W bosons produced in 13 TeV pp collisions using prompt and displaced signatures with the ATLAS detector*, *JHEP* **10** (2019) 265, [[1905.09787](#)].
 - [59] C.-W. Chiang, G. Cottin, A. Das and S. Mandal, *Displaced heavy neutrinos from Z decays at the LHC*, *JHEP* **12** (2019) 070, [[1908.09838](#)].
 - [60] CMS collaboration, A. M. Sirunyan et al., *Search for Evidence of the Type-III Seesaw Mechanism in Multilepton Final States in Proton-Proton Collisions at $\sqrt{s} = 13$ TeV*, *Phys. Rev. Lett.* **119** (2017) 221802, [[1708.07962](#)].
 - [61] ATLAS collaboration, M. Aaboud et al., *Search for doubly charged Higgs boson production in multi-lepton final states with the ATLAS detector using proton-proton collisions at $\sqrt{s} = 13$ TeV*, *Eur. Phys. J.* **C78** (2018) 199, [[1710.09748](#)].
 - [62] CMS collaboration, C. Collaboration, *A search for doubly-charged Higgs boson production in three and four lepton final states at $\sqrt{s} = 13$ TeV*, .
 - [63] ATLAS collaboration, M. Aaboud et al., *Search for doubly charged scalar bosons decaying into same-sign W boson pairs with the ATLAS detector*, *Eur. Phys. J.* **C79** (2019) 58, [[1808.01899](#)].
 - [64] MoEDAL collaboration, B. Acharya et al., *The Physics Programme Of The MoEDAL Experiment At The LHC*, *Int. J. Mod. Phys.* **A29** (2014) 1430050, [[1405.7662](#)].
 - [65] MoEDAL collaboration, B. Acharya et al., *Search for magnetic monopoles with the MoEDAL forward trapping detector in 2.11 fb^{-1} of 13 TeV proton-proton collisions at the LHC*, *Phys. Lett.* **B782** (2018) 510–516, [[1712.09849](#)].
 - [66] C. Arbeláez, J. C. Helo and M. Hirsch, *Long-lived heavy particles in neutrino mass models*, *Phys. Rev.* **D100** (2019) 055001, [[1906.03030](#)].
 - [67] R. Cepedello, M. Hirsch and J. C. Helo, *Lepton number violating phenomenology of $d = 7$ neutrino mass models*, *JHEP* **01** (2018) 009, [[1709.03397](#)].
 - [68] R. Cepedello, M. Hirsch and J. C. Helo, *Loop neutrino masses from $d = 7$ operator*, *JHEP* **07** (2017) 079, [[1705.01489](#)].